

NAT'L INST. OF STAND & TECH R.I.C.



A11105 355206

REFERENCE

NIST
PUBLICATIONS

NISTIR 6017

Optical Pattern Recognition with Microlasers

Eung Gi Paek

Information Technology Laboratory

U.S. DEPARTMENT OF COMMERCE
Technology Administration
National Institute of Standards and Technology
Gaithersburg, MD 20899-0001

QC
100
.U56
NO.6017
1998

NIST

Optical Pattern Recognition with Microlasers

Eung Gi Paek

Information Technology Laboratory

U.S. DEPARTMENT OF COMMERCE
Technology Administration
National Institute of Standards and Technology
Gaithersburg, MD 20899-0001

January 1998



U.S. DEPARTMENT OF COMMERCE
William M. Daley, Secretary

TECHNOLOGY ADMINISTRATION
Gary R. Bachula, Acting Under Secretary for Technology

NATIONAL INSTITUTE OF STANDARDS
AND TECHNOLOGY
Raymond G. Kammer, Director

Optical pattern recognition with microlasers

Eung Gi Paek

Optical pattern recognition has existed for approximately 45 years. The computational power of optics to perform 2-D (two-dimensional) Fourier transform, convolution and correlation at the speed of light is certainly unique over other technologies. Many different system architectures have been demonstrated to utilize the merits of optics.

However, the evolution of optical pattern recognition has been rather slow and its performance often has been challenged by its counterpart, digital computers. This was mainly due to the lack of suitable input/output devices such as SLMs (spatial light modulators) and detectors available in the market. Most of the input/output devices were developed for other consumer applications and their speeds were usually limited to conventional video rates (30 frames per second). With the rapid advances in digital computers that can perform near-video-rate 2-D Fourier transformation, higher speed devices are desperately needed in optical information processing.

New device possibilities exist in optical pattern recognition and information processing. Recent advances in optoelectronic device technology include surface emitting microlaser arrays, among others, which have a great potential for ultra-high speed (more than two orders of magnitude faster than video rate) optical pattern recognition and ATM header recognition due to their parallel computing capability.

The current status of the microlaser technology will be briefly reviewed and possible applications of new devices for optical pattern recognition and information processing will be described. Advances in these technologies would contribute to the underlying device infrastructure needed for advanced communications services, such as those sketched by the National Information Initiative or "information superhighway".

12.1 Introduction: microlasers, surface emitting laser diode arrays, or vertical-cavity surface emitting lasers

12.1.1 What is a surface emitting laser ?

Fig. 12.1 compares the surface emitting laser (SEL) diode [Fig. 12.1(a)] with the conventional edge emitting semiconductor diode laser in a compact-disc player [Fig. 12.1(b)]. In a conventional edge emitting laser diode, the laser beam emerges parallel to the active layer. Therefore a two-dimensional (2-D) arrangement of lasers is difficult. In contrast, the light from a SEL diode emerges perpendicular to the active layer, allowing a 2-D stack of many lasers on a planar wafer substrate. Iga and his co-workers first proposed and demonstrated the feasibility of such SEL diodes in the late 1970's [1,2].

Fig. 12.1. (a) Vertical cavity surface emitting microlaser, (b) edge emitting diode laser. (Reprinted from Ref. [4] by Jewell et al.)

12.1.2. What is a microlaser?

The original SEL's had a relatively large active volume (typically $10 \mu\text{m}^3$), requiring a large driving current. In May 1989, a miniaturized surface emitting microlaser with a very small active volume (typically $0.05 \mu\text{m}^3$) than that of previous SEL's was developed [3-7]. As can be seen in Fig. 12.2, a small hairlike structure with a diameter of only $1.5 \mu\text{m}$ is an independent laser. The hairlike structure consists of an active layer surrounded by a pair of high-reflectivity mirrors on both sides. The laser cavity is formed along the direction normal to the wafer surface and laser light is emitted in either the top or the bottom direction. Therefore such lasers are often called vertical cavity surface emitting lasers (VCSEL's) to differentiate them from other surface emitting lasers that have the cavity along the wafer surface.

The small size of the active layer of the device, which consists of very thin (approximately 100 \AA) quantum well layers, requires a very low driving current to turn on the laser. To compensate for the low gain through the thin active region, the resonators at both ends of the active medium should have extremely high reflectivity to minimize losses, typically 99.9% or a finesse of 3000. This high-reflectivity mirror and the efficient confinement of both electrons and

photons within a waveguide define the two major difficulties in fabricating microlasers. We call such an array of microlasers a surface emitting laser diode array (SELDA), or microlasers, in addition to the more commonly used term, VCSEL.

Fig. 12.2. Scanning electron micrographs of vertical cavity surface emitting microlasers. (VCSEL's, SELDA's or microlasers) (Reprinted from Ref. [4] by Jewell et al.)

12.1.3 Why microlasers?

The microlaser has many good features that make it an excellent candidate for optical information processing. Some of the important features include:

- Individual microlasers can be as small as a few micrometers. In addition, the surface emitting features allow 2-D integration of many lasers. Therefore approximately 10^6 lasers can be arranged in a 1 cm^2 chip area.
- Because of the small volume of the active medium, the threshold current can be very low (up to a few microamperes), greatly reducing the power requirements of a system (compared with edge emitters, whose threshold currents are 5 mA to 20 mA).
- The spectral linewidth of a microlaser is very narrow, typically less than 0.01 nm, for reasons that are explained below. Therefore a microlaser has a longer coherence length than a conventional Fabry Perot laser diode.
- The beam profile of a microlaser is naturally circular. Therefore the beam can be directly used to illuminate optical components or spatial light modulators (SLM's) without requiring anamorphic prisms or lenses as in edge emitting lasers. In this way, a conventional gas laser and a pinhole spatial filter can be replaced by a simple microlaser, making a compact and robust system.
- The manufacturing and test process of a microlaser is simple, once the crystal growth step is completed. Millions of microlasers can be obtained simultaneously. Moreover, microlasers can be easily tested in wafer form, whereas edge emitters must be cleaved before testing. Therefore microlasers have a potential for low-cost mass production.

Table 12.1 lists some of the differences between edge emitters and surface emitters.

However, current microlasers have the following limitations:

- The wavelengths of the microlasers are mostly limited to 0.75 μm - 1.0 μm . Therefore a holographic recording with a microlaser is currently difficult because most of the holographic recording materials are sensitive to visible wavelengths.
- Polarization of a microlaser is random or uncontrollable. This problem can be solved in a controllable manner by use of various methods, as explained in subsection 12.2.5.
- The output power of a microlaser is not as high as that of an edge emitting laser diode.
- The microlaser is still in its infancy; therefore extensive studies of packaging, addressing, and reliability are few compared with those of edge emitters.

Nonetheless, the microlaser is certainly one of the most important photonic devices developed in this decade and will play an increasingly important role in the future of optical information processing. Currently, active research is being pursued over the world to overcome these problems.

12.2 Status of microlasers

Below, the current status of microlasers related to optical information processing is summarized.

12.2.1 Low threshold current

An important parameter used to characterize the power requirements of any diode laser is its threshold current, the minimum current needed for lasing. A low threshold current of 8.7 mA single quantum well [8] and a low threshold voltage 1.33V VCSEL grown by metal-organic chemical vapor deposition (MOCVD) were demonstrated [9]. An extremely large power conversion efficiency of over 50% was also achieved [10]. Also, a microlaser with a threshold current density of 80 A/cm^2 was demonstrated.[11]. An ultralow low threshold operation can be

expected with reduction in the active region volume until we meet the limitation that is due to nonradiative recombination, and optical and electrical confinement [11,12].

A thresholdless microlaser that does not have a threshold current like a light emitting diode (LED) but still possesses narrow linewidths by photon recycling has also been reported [13].

12.2.2 Coherence

Coherence is one of the most important attributes of a light source for optical information processing and pattern recognition. The spectral linewidth of a microlaser is very narrow [14-16]. This narrow linewidth is attributed to the short cavity length of the microlaser that can support only a single longitudinal mode, an effect similar to that of a distributed-feedback (DFB) laser or a gas laser with a Fabry Perot etalon. In addition, the high reflectivity of the reflector functions as a spectral filter. Therefore a microlaser has a longer coherence length than a conventional Fabry Perot laser diode (See Table 12.1). A short linewidth of 65 MHz has been measured with heterodyne techniques for a microlaser (850 nm to 865 nm wavelengths) operated near threshold [15]. This corresponds to a coherence length of 5 m (0.00014nm linewidth) and is comparable with that of an Ar-ion laser with an etalon.

Although microlasers operate inherently at a single longitudinal mode, the coherence length still decreases at high current levels. This is due to the multiple transverse modes at high currents. Fig. 12.3 illustrates output light power versus current (L-I) and voltage versus current (V-I) curves for a typical top-surface emitting gain-guiding microlaser [18]. The apparent kinks in both curves are associated with changes in the optical mode and corresponding carrier distributions. The first threshold corresponds to the TEM_{00} lasing mode. The first plateau in the L-I characteristic is associated with the saturation of the TEM_{00} mode. The subsequent threshold corresponds to the onset of the TEM_{01} mode. Lasing begins in the TEM_{00} mode, but further increases in the current result in the occurrence of additional higher order transverse modes. These higher-order transverse modes generates additional spectral modes that are typically separated by approximately 0.7 nm, which greatly reduces the coherence length and the beam profile of an expanded beam.

Such a problem was solved with a spatial filtering technique, which was achieved by a simple reduction in the contact aperture size with respect to the width of the confinement (surrounded by

the implantation) [18]. In this way, the kinks were eliminated and a single transverse mode operation leading to a high coherence length was achieved even at high current levels without sacrificing the output power (approximately 63%) too much.

Also, each laser of the array operates independently; they are not phase locked with each other [19].

Fig. 12.3. Light output power versus current and voltage versus current curves of a typical microlaser. (Reprinted with permission from Ref. [18] by Morgan et al., © 1993 IEEE.)

12.2.3 Visible microlasers

Current microlasers operate mainly in the wavelength range of 0.75 μm -1.0 μm which can be achieved with GaAs-based alloys. However, researchers are developing shorter-wavelength microlasers. This is motivated by the fact that the shorter wavelength would allow a larger capacity of an optical storage medium as well as easy alignment. The visible operation is crucial particularly for holographic information processing because most holographic recording materials are sensitive to only visible wavelengths.

The main difficulty in the fabrication of visible microlasers lies in the creation of mirrors with high reflectance and low loss in the visible region. Room-temperature lasing to wavelengths as short as 0.63 μm was demonstrated with InGaAlP alloys [20-23].

Recently an electrically pumped blue microlaser array was also demonstrated [24,25]. Laser action was achieved at a wavelength of 484 nm under a pulsed-current injection at 77 K. The microlaser structure was composed of a CdZnSe/ZnSe multiple-quantum-well active layer, ZnSe cladding layers, and $\text{SiO}_2/\text{TiO}_2$ distributed Bragg reflectors (DBR's). This result shows promise of the microlaser for holographic information processing based on photorefractive crystals, many of which are sensitive at blue-green wavelengths. Likewise, additional work on blue-green lasers with homoepitaxial deposition of ZnSe is currently being pursued.

The recent demonstration of a blue laser diode by Nakamura at Nichia Chemical Ind. Ltd. (Tokushima, Japan) [26] shows great promise in the blue-green operation of the microlaser. The laser is II-VI based (GaN material with InGaN multiple quantum wells) and is currently operated at room temperature in a pulsed mode at 390 nm to 440 nm for an edge emitting structure.

12.2.4 Two-dimensional addressing schemes

In a SELDA, more than 10^6 lasers are available in a 1 cm X 1 cm area. A major issue in operating such devices is their addressing scheme. Three different approaches have been developed for 2-D addressing: individual addressing, matrix addressing, and optical addressing.

Individual addressing is the most straightforward method and uses an independent wire for each microlaser. This requires a tremendous amount (N^2 , where N is the number of lasers along one direction) of wires and pads and becomes impractical as N becomes large. Several individual addressing schemes have been demonstrated [27].

Matrix addressing is the scheme most commonly used to address 2-D devices such as liquid crystal displays or dynamic random access memories (DRAM's). All the SEL's in the same row (or column) are connected together with their common external wire pad. These rows and columns are on the opposite side of the SEL's. To turn on a particular SEL at (i, j) , a voltage is applied across the i -th row and the j -th column pad. This point-by-point addressing can be easily extended to line-by-line addressing by the simultaneous application of voltages across all the columns and a row. Such a matrix-addressing scheme requires only $2N$ electrodes and is easy to fabricate. A monolithic 32 X 32 matrix addressable SELDA has been demonstrated by Orenstein et al., as shown in Fig. 12.4 [28]. Recently a high-density array of microlasers with a spacing of 30 μm between neighboring lasers was demonstrated [29].

Fig. 12.4. Matrix addressing of a microlaser array. (Reprinted with permission from Ref. [28] by Orenstein et al., © 1991 IEE.)

Finally, an optical addressing scheme of a SELDA is shown in Fig. 12.5. In this device, a 2-D image illuminating one side of a SELDA is detected by an array of heterojunction phototransistors (HPT's), and the current generated by each HPT turns on the corresponding laser. This method allows a complete parallel load of an image, without the need for electrical connections. A monolithic array of such an optically addressable SELDA has been demonstrated [30]. A similar concept had been developed for LED's by various groups and was used for

optical information processing [31-33]. The output-light versus input-light relationship is described below in Subsection 12.5.2.

Fig. 12.5. Optically addressable integrated SELDA: (a) structure of the device, (b) light-output versus light-input relationship. (Reprinted with permission from Ref. [30] by CHAN ET AL., APPLIED PHYSICS LETTERS, 58, 2342-2344, 1991. © 1991 American Institute of Physics.)

12.2.5 Polarization control

The output light from a microlaser is not linearly polarized. Therefore polarization control is one of the most important subjects to be resolved, especially for polarization-sensitive applications such as magneto-optic disks and coherent detection systems. Recently it was theoretically and experimentally predicted that the polarization of a microlaser grown on an (n11)-oriented substrate could be simply controlled by use of its intrinsic in-plane anisotropic gain distribution characteristics [34]. Stable polarization characteristics based on the prediction were realized for a conventional microlaser structure [35].

12.2.6 Multiple wavelengths

Multiple wavelengths and tuning are highly desirable in optical information processing and communications. A 2-D multicolor SELDA (MC-SELDA) is a 2-D array of microlasers, each with its own wavelength. Fig. 12.6(a) shows a monolithic 2-D MC-SELDA originally demonstrated by Chang-Hasnain et al. [36]. The 7 X 20 array has a total of 140 microlasers, and each laser has a unique wavelength that is uniformly separated from its neighbors by 0.3 nm, spanning a total wavelength of 43 nm. Such a wavelength variation was obtained by varying the laser cavity lengths when growing the wafers as shown in Fig. 12.6 (b).

More recently, the same group demonstrated a record wavelength span of 62.7 nm by using a modified patterned-substrate growth technique in a molecular beam epitaxy system [37]. The authors claim highly uniform threshold currents with an average of approximately 2 mA with a high repeatability of wavelength spacing and a sharp wavelength-shift rate of 117.14 nm/mm.

Fig. 12.6. 2-D MC-SELDA: (a) device, (b) wafer. (Reprinted with permission from Ref. [36] by Chang-Hasnain et al., © 1991 IEEE.)

12.2.7 Wavelength tuning

Continuously tunable lasers have a huge number of potential applications. These range from free-space optical interconnects and wavelength-division multiplexing for communications to holographic data storage and spectroscopy. The microlasers can be tuned in the same way as for edge emitting lasers by varying the drive current applied to them. Recently a new method of wavelength tuning based on a deformable membrane mirror has been demonstrated [38]. As shown in Fig. 12.7, the mirror is fabricated at the end of a light emitting cavity, with a small air gap separating the two. As the mirror moves back and forth, the length of the cavity changes, resulting in a change in the resonant wavelength. A tuning range of 15 nm has been demonstrated using the method. Currently, the device requires extremely high threshold current, 37 mA to 64 mA and thus had to be operated in pulsed mode, rather than continuous wave.

Fig. 12.7. Wavelength tuning of a microlaser by a deformable membrane mirror. (Reprinted with permission from Ref. [38] by Wu et al, © 1991 IEE.)

12.2.8 Efficiency

High electrical-to-optical power conversion (wall-plug) efficiency is one of the most important parameters for estimating power consumption. Microlasers suffer from poor wall-plug efficiencies because of excessive voltage drops across the DBR's. However, recent overall cw power efficiencies have approached 20% [39]. Also, dramatic improvements in microlaser power conversion efficiency of up to 50% at low currents have been realized [40] with an index-guided top-emitting structure based on selective oxidation. The efficiencies demonstrated are at least comparable with those of edge emitting lasers.

12.2.9 Modulation speed

The injection current modulation bandwidth of small microlasers has been predicted to be very high (>100 GHz) for the following reasons [41] :

- For a give injection current, the small volume of a microlaser leads to a large photon density and hence a short stimulated lifetime.

- Cavity quantum electrodynamic effects have been expected to increase the differential gain, because of an enhancement of the emission rate into the lasing mode. Recent measurements indicate a fast intrinsic response, with a 3-dB modulation bandwidth of more than 50 GHz [42].
- Recent analyses indicate that a microlaser, under the constraint of nonlinear gain or current density limitations, has the same intrinsic modulation bandwidth as conventional edge emitting lasers with the same cavity losses and photon density [43]

12.2.10 High power output

In spite of the small size of the microlaser, it can be operated at reasonably high power levels. A cw output of more than 100 mW with a wall plug efficiency of 20% has been demonstrated by a group at the University of California at Santa Barbara; they tailored the laser's operation to increased temperatures [44]. Also, 1-W pulsed operation has been demonstrated with a top-surface emitting 100 μm X 100 μm broad-area laser with a grid contact segregating the laser into a 10 X 10 array of 8 μm X 8 μm emission windows [45].

12.3 Optical correlators with microlasers

12.3.1 Introduction

Pattern recognition has long been one of the major applications of optics. The capability of computing a complicated operation, such as a 2-D Fourier transform, convolution, and correlation based on the wave nature of optics, has provided a strong tool for this application. Correlation is an operation that calculates the similarity of two patterns and is widely used for pattern recognition. It is represented by an equation $g(x, y) = \iint f(\xi, \eta) \cdot h(\xi - x, \eta - y) d\xi d\eta$, where f , h and g refer to an input, a filter, and a correlation output, respectively. Therefore summation and shift are two basic operations in calculating correlations.

12.3.2 Classification of optical pattern recognition systems

Optical correlators have been around since the early 1950's. Although most of the current optical correlators are based on the coherent optical processors (either the VanderLugt or the joint transform correlator), there are many other types of correlators, as is shown in Fig. 12.8. Below, a brief description of each of the systems is provided. More detailed analyses can be found in various Ref's [46-48].

Fig. 12.8. Classification of optical correlators. TDI, time delay and integration.

(1) Kretzmer-type correlator [49]: This is probably the oldest and most straightforward correlator developed in the early 1950's. In the system, summation is achieved spatially by an optical lens and is detected by a single detector. Also, a shift operation is achieved by one (or both) of the inputs is mechanically moved along both the x and the y directions. Such a movement can be achieved by an acousto-optic beam deflector in which the signal flows through the one-dimensional medium. Unfortunately, there are no fast 2-D image shifters, currently.

(2) Shadow casting [50-52]: In this system architecture, both shift-and-add operations are done in an all-optical fashion simultaneously. The problems with such a system are diffraction effects and no room for the spatial filtering operation. Microlasers, even with their natural 2-D nature, can find limited application for this type of correlator because of the diffraction effect that is due to the high coherence of the light from microlasers.

(3) Electro-optic correlator with a time-delay-and-integration-mode CCD [53,54]: In this system, an input signal $f(t)$ is temporal and is emitted from a point source such as an LED or a laser diode. The reference signal $h(x)$ is recorded in an SLM that is in contact with (or imaged to) a time-delay-and-integration-mode CCD sensor. Both the input signal and the CCD are synchronized and systolically perform the shift-and-add operation to calculate the correlation.

(4) Electro-optic correlator with a normal CCD: This system is equivalent to the system in (3) except that the time-delay-and-integration-mode CCD is replaced by a moving reference signal and a normal CCD.

(5) VanderLugt correlator [55]: This architecture has probably been the most commonly used architecture for optical pattern recognition. Pattern recognition is achieved in two steps: (1) holographic filter fabrication and (2) processing. In the first holographic filter fabrication step, a matched filter for a given reference image is holographically fabricated with the Fourier transform holographic recording technique. In the processing step, if an input matches the reference image, the wave-front distortion generated by an input pattern is canceled out and a plane wave is generated. The plane wave is then focused to a point at the focal plane of the second lens.

The system has been successful because of the high signal-to-noise ratio (SNR) that can be achieved with additional spatial filtering that can be easily achieved in the system. Also, once a holographic filter is fabricated, it is fully nonblocking without requiring a photon-to-electron conversion process that can lead to speed bottleneck.

However, the system requires an input from high-optical-quality recording materials and a holographic filter to preserve shift-invariant recognition. The filter has to be positioned exactly in the original position in which it was recorded. Also, the holographic filter must be positioned exactly in the focal plane of the Fourier transform lens. Recent advances in high-quality SLM's and in situ holographic recording materials allow a convenient implementation of such an optical correlator with high performance.

(6) Joint transform correlator [56,57]: The joint transform correlator has become popular these days because it is simple to implement and real-time operation is possible with currently available devices (SLM's and 2-D CCD's) [58].

The operation of the joint transform correlator can be considered a two-step Fourier spectrum (modulus square of a Fourier transform) generation. At first, both an input and a reference image are located in the input plane (spatial domain) side by side. The Fourier spectrum of the two inputs is recorded in a high-resolution recording material. The Fourier spectrum of the two inputs is Fourier transformed again by the second Fourier spectrum generator. The first order diffraction outputs from the second Fourier spectrum generator are the correlations of the input and the reference images.

Optics can perform a real-time Fourier spectrum generation quite well in a simple and low-cost setup consisting of a laser, an SLM, a 2-D image sensor, such as a CCD, and a spherical lens.

The advantages of the system are that it allows easy real-time implementation of a correlator with currently available devices and it does not require accurate filter positioning. Also, as in a VanderLugt correlator, various spatial filtering operations such as bipolar phase-only filtering can be incorporated [59-61]. Moreover, one can use different wavelengths for hologram recording and readout without requiring careful alignment.

The disadvantages are that it requires a fast and high resolution holographic recording material and the correlator is not all-optical, requiring intermediate photon-to-electron conversion processes.

The recent photorefractive semi-insulating multiple-quantum-well SLM developed by A. Partovi et al. [62] has many desirable features suitable for such correlators. It has high speed (a several microseconds for 280 mW/cm^2 at $600\text{nm} - 850 \text{ nm}$), high sensitivity ($0.8 \mu\text{J/cm}^2$ to allow the use of a low power laser diode), high efficiency (3%), low operational voltage (20 V), a large index change (0.06), and a reasonable resolution (50 lines/mm). A high-speed joint transform correlator that uses this device has been successfully demonstrated [63]. The system uses a low power laser diode (3 mW) and is capable of 3×10^5 correlations/s. When the system is incorporated with a fast ferroelectric liquid crystal SLM and a fast detector, several thousand correlations can be achieved within a second. This speed is about two orders of magnitude faster than that of digital computers.

Although the above correlators are described in one-dimensional terms, many combinations of the above architectures are possible [64,65]. The classical holographic pattern recognition system in (5) has had limited application because it is bulky and is too sensitive to misalignment, input recording materials, and filters. Such problems can be greatly alleviated with a SELDA. Two recently developed correlators based on microlasers are introduced below.

12.3.3 Multichannel optical correlator based on a mutually incoherent microlaser array

Yang and Gregory [66] demonstrated a multichannel optical correlator by using the mutually incoherent property of a microlaser array to improve the performance of an optical correlator with respect to immunity to coherent noise and a high SNR as well as high light throughput. As shown in Fig. 12.9, an optical correlator is incoherently duplicated by an array of light sources to increase the SNR.

Fig. 12.9. Multichannel optical correlator with a mutually incoherent microlaser array. FT, Fourier transform. (Reprinted from Ref. [66] by Yang and Gregory, © 1995 Optical Society of America.)

In the system, the Fourier spectra due to different microlasers can overlap one another if the separations between neighboring microlasers are adjusted to match the period of an SLM in the filter plane. Although a matched filter was synthesized with a single reference pattern, it is duplicated at many periodic locations in the Fourier plane and matches the multiple input spectra. In this way, an efficient space-bandwidth product in the filter plane is increased and sharper correlation peaks are obtained.

Such an approach would be extremely useful for increasing the reliability of a conventional optical correlator. The only practical issues here are generation of reference beams that are coherent with object beams to record holograms and the removal of undesired fringes in an autocorrelation peak. The authors suggested a time-division-multiplexing (TDM) scheme as a way to eliminate interference fringes.

12.3.4 Compact and robust incoherent correlator

As explained above, the light from a microlaser is highly monochromatic. However, the phases of the light from the microlasers are not locked with each other. These two unique coherence properties (temporally highly coherent and spatially incoherent) make a SELDA an ideal light source for implementing a compact and robust incoherent correlator.

Fig. 12.10. Compact and robust incoherent correlator: (a) system, (b) experimental results.

Fig. 12.10 (a) shows an example of the microlaser-based incoherent correlator [67]. The light from each SEL is collimated by lens L_1 and illuminates the hologram to reconstruct holographic images on the output plane which is located at the focal plane of lens L_2 . The image generated by each SEL is shifted by the amount that corresponds to the position of the SEL. The reconstructed images generated by the light from different SEL's are added up incoherently because each laser operates independently, averaging out the phase-sensitive interference terms. The eventual summation of all the reconstructed images generated by all the SEL's in the input plane gives the correlation between the input and the reference image stored on the hologram. Because the system does not involve any moving parts (e.g., rotating diffuser) or bulky optical components, the whole system can be miniaturized and integrated with semiconductor technologies.

Fig. 12.10 (b) shows the correlation output obtained from the SELDA correlator. A holographic filter was fabricated for the input pattern (Bell logo) and was tested for the two input patterns (the Bell logo and a Chinese character meaning light). For the correct input [Bell logo (middle)], a bright autocorrelation peak appears at the center of the correlation output (middle, right). On the other hand, for the incorrect input [Chinese character (bottom)], a cross-correlation is obtained (bottom, right). As shown in the figure, the cross-correlation signal is much weaker than the autocorrelation peak, allowing a satisfactory discrimination between the two input patterns.

12.4 Holographic memory readout with microlasers

12.4.1 Introduction

Volume holographic memory has been extensively investigated in the past as a way of massively storing media to allow fast random access page-organized memory [68-72]. This volume holographic memory has reawakened its interest recently because of the immense demand for storage media with fast access and a large storage capacity for applications such as multimedia. However, the holographic system normally requires bulky and complicated beam deflectors to steer the beam direction from one to another, corresponding to the desired page. Moreover, speed and resolution of a beam deflector are quite limited.

12.4.2 Compact and ultrafast holographic memory with a SELDA

Such traditional problems can be solved with a SELDA[73]. As is explicitly shown in Fig. 12.11, a SELDA combined with a simple collimating lens can function as an efficient multiple beam steerer to change the beam direction from one to the other. Such beam steering can be achieved within one nanosecond, compared to the switching speed of the microlasers. This ultrafast beam steering is used to reconstruct angular-multiplexed holographic memories in which each image is recorded using the second beam (reference beam) propagating along a different angle. By using this simple and compact optical setup, any frame can be randomly accessed within one billionth of a second.

Fig. 12.11. Compact and ultrafast holographic memory with a microlaser array.

In the experimental results shown in Fig. 12.11, memories are recorded in a volume hologram (LiNbO_3 crystal, 0.01% Fe doped) that can provide a large storage capacity of around ten billion bits because of the third dimension available in a volume storage medium. The figures on the right-handed side show the images retrieved from the volume hologram by the light from a SELDA. Each laser is separated from the adjacent one by $70\ \mu\text{m}$, corresponding to an angular separation of about 0.04° . As can be seen in the figure, the two independent lasers separated by only $70\ \mu\text{m}$ reconstruct totally different images. In this way, each tiny microlaser can be matched to a separate page, allowing the array to form a selective address generator.

12.4.3 Combined angular and wavelength multiplexing with a two-dimensional MC-SELDA

In general, angular multiplexing can be achieved along one direction in a plane formed by both reference and object beam directions because of the degeneracy effect. As can be seen in Fig. 12.12 (a), the Bragg condition is satisfied by waves that have any of the directions that form the surface of a cone (the shaded area in the figure) whose axis is normal to the grating planes [74]. This degeneracy causes cross-talk along the direction perpendicular to the Bragg direction. However, this cross-talk can be greatly reduced by use of different wavelengths along the degenerate directions, as shown in Fig. 12.12(b). Such a concept has been recently demonstrated

with five different wavelengths to record a total of 2000 holograms: five different wavelengths with 400 angularly multiplexed images for each wavelength [75].

Fig. 12.12. Breaking degeneracy by use of multiple wavelengths.

The concept can also be implemented in a compact and ultrafast fashion by a 2-D MC-SELDA, as shown in Fig. 12.13. The SELDA has the same wavelength along the angular-multiplexing direction and different wavelengths along the degeneracy direction. In addition, such a combinational multiplexing with a MC-SELDA has an additional angular separation effect along the degenerate direction because each microlaser lies in a different position. In this way, the storage capacity of a volume hologram can be greatly increased in a compact and ultrafast readout system within the total limit imposed by the available number of charge carriers in a medium and the theoretical limit of V/l^3 , as is proved by Lee et al. [76] and Psaltis et al. [77].

Fig. 12.13. Compact and ultrafast holographic memory readout with 2-D (Angle + Wavelength) multiplexing by a 2-D MC-SELDA.

12.4.4 Incoherent /coherent multiplexing with a SELDA

An incoherent /coherent multiplexing approach to reduce the noise due to multiplexing by use of an array of microlasers has been developed by Jenkins and Tanguay [78]. The concept of the method can be understood as follows:

When multiple gratings are recorded simultaneously by a coherent light source, all the cross terms are added coherently. In other words, the amplitudes of all the gratings are summed first and squared later. As a result, the number of noise gratings (or the number of cross-talk terms) becomes N^2 , where N is the number of gratings. On the other hand, as in this proposed method, if each grating is recorded sequentially one by one, the cross-terms are incoherently added (each grating amplitude is squared first and summed over all the gratings later), and thus the number of noise gratings becomes N ; therefore cross-talk can be greatly reduced. Such an incoherent recording can be achieved simultaneously with an array of independent (not phase locked with each other) coherent light sources, such as an SELDA. Jenkins and Tanguay applied this noise

reduction method to photonic interconnection and holographic optical elements for 2-D wavelength-division multiplexing applications.

This technology of using microlasers for holographic storage will be extremely useful when suitable holographic recording materials become available in the future. Recent developments in biological holographic recording materials, such as bacterial rhodopsin, show a great new promise for future computers [79].

12.5 Microlasers for holographic associative memory

12.5.1 Introduction

Recent advances in neural networks opened many new possibilities for optical information processing for broad application areas [80-82]. Optics, especially coherent optics, has found an excellent match in implementing the neural networks that require parallel and analog computing.

Fig. 12.14 illustrates an associative memory for word-break recognition to generate a readable text from a continuous string of words. In the system, an input word stream is presented at the input plane of the system. Autocorrelation peaks that appear at places where there is a match between the input and the memory words pre-recorded in a hologram are detected. All the spurious sidelobes are removed by a threshold operation in the correlation plane. Next, the separation between the peaks is magnified along the word direction. This stretched correlation output is reflected back to illuminate the hologram and reconstruct the whole memory at the output plane. The output through a window that is situated at the origin of the output plane is the desired readable text, with all the errors corrected and spaces inserted between words.

Fig. 12.14. Holographic associative memory for word-break recognition.

12.5.2 Holographic neurons

Such a neural network system normally consists of three parts: (1) a recognition part to compare an input with all the memories, (2) a reconstruction part to retrieve the corresponding memory, and (3) nonlinear thresholding elements to make decisions. Recognition (pattern recognition in

subsection 12.3.2) and reconstruction (holographic memory in 12.3.1.) have already been described. Below, we focus on the third part, nonlinear thresholding elements, or so called optical neurons.

There has been much research done on optical neurons. Recently an integrated vertical-cavity surface emitting microlaser array with HPT's to yield optically controlled lasers has been demonstrated by Chan et al.[30]. The structure of the device is shown in Fig. 12.5, as explained above. Fig. 12.5(b) shows the output versus input optical power relationship for various bias voltages. As shown in the figure, the device displays a suitable nonlinear threshold function as an optical neuron with the threshold input optical power of 0.1 mW (at the wavelength of 855 nm). It also provides an optical gain of approximately 5, making it an excellent candidate for an optical neuron array.

Besides its nonlinear threshold function, the output light from the optical neuron is coherent. It is a laser; therefore, it can reconstruct any type of hologram. In Fig. 12.15(a), the neuron with an input power above threshold is fired to reconstruct the corresponding memory. Fig. 12.15(b) shows an experimental result. If the output light signal is below threshold, nothing appears in the output plane (left). On the other hand, as soon as the input light is increased above the threshold level, the neuron is fired and the corresponding holographic memory is retrieved (right).

Fig. 12.15. Holographic memory readout with an array of holographic neurons: (a) system, (b) experimental results.

12.5.3 Microlaser-based holographic associative memory

When the optical neurons are combined with both recognition and reconstruction parts, which were demonstrated above, in a simple two-lens system, a compact, ultrafast, and highly efficient neural network system may be implemented in the future. Furthermore, the bulk lenses can be replaced by planar zone plates, allowing the integration of the whole system into the smallest scale possible.

in this approach. This is even more serious in this case than in conventional diffractive optical components in free-space optics because the light path length is short and all the other components need to be scaled down accordingly.

A hybrid integration of a microlaser chip and a planar optics substrate has been implemented [89]. In the system, a top-surface emitting microlaser array (9 μm diameter, 85 μm spacing, and 850nm wavelength) was bonded to a single quartz glass substrate by the flip-chip bonding technique with indium solder bumps. The lenses were lithographically fabricated by the diffractive optical element technique with four phase levels. They have a square shape with a size of 500 μm X 500 μm . Their focal lengths match the thickness of the glass substrate, which is 3 mm. Surrounding areas are coated with a Ge film to absorb any undesired stray light. The deflection angle relative to the normal is limited by the resolution of the lithographic process; it was 6.2° in this experiment.

Various other approaches along similar lines have been proposed and implemented [91-93].

12.7 Conclusion

Optical pattern recognition has often been superseded by the rapidly growing digital computer technology that approaches near-real-time processing. However, it should be noted that the computational power of optics to compute 2-D Fourier transformation, convolution, and correlation at the speed of light is still unique and is not expected to be surpassed by other technologies. Even with current device technologies, optical pattern recognition can achieve more than 1,000 image comparisons per second. Extrapolating the developmental speed of digital computers doubling every two years, 1000 high resolution image comparisons per second (about two orders of magnitude faster than what is available now) would require another 15 years or so and will not be attained by the year 2010. Before then, the explosion of information in the form of multimedia through the internet will increasingly demand faster and faster image comparisons and understanding, for which optical pattern recognition can provide many opportunities.

Fortunately photonic technology forms the backbone of the current communication technology. The current transmission speed of an optical signal is moving beyond 1 THz, much

faster than the clock speed of a digital computer. Total available optical bandwidths can be as high as 25 THz at the communication wavelengths. These bandwidths give a clear edge to optics-based information technology for storage, displays, and processing. In this regard, optical pattern recognition has a bright future if it is closely tied to other photonic technologies and takes advantage of new photonic devices. For example, the developmental speed of SLM's has been much slower than that of photonic devices for communications.

Undoubtedly, surface emitting microlasers will have rich new possibilities for pattern recognition as the device technology becomes mature enough to allow low (of the order of microwatts) power consumption per laser, high reliability, integration with other devices, and suitable addressing schemes for high density arrays, etc.

Current optical pattern recognition systems need to be greatly improved in terms of not just speed but of accuracy. This accuracy requires the development of elaborate measurement methods to calibrate and test performances. Such test and measurement issues need to be seriously addressed in the future before any optical systems are to be used for practical purposes.

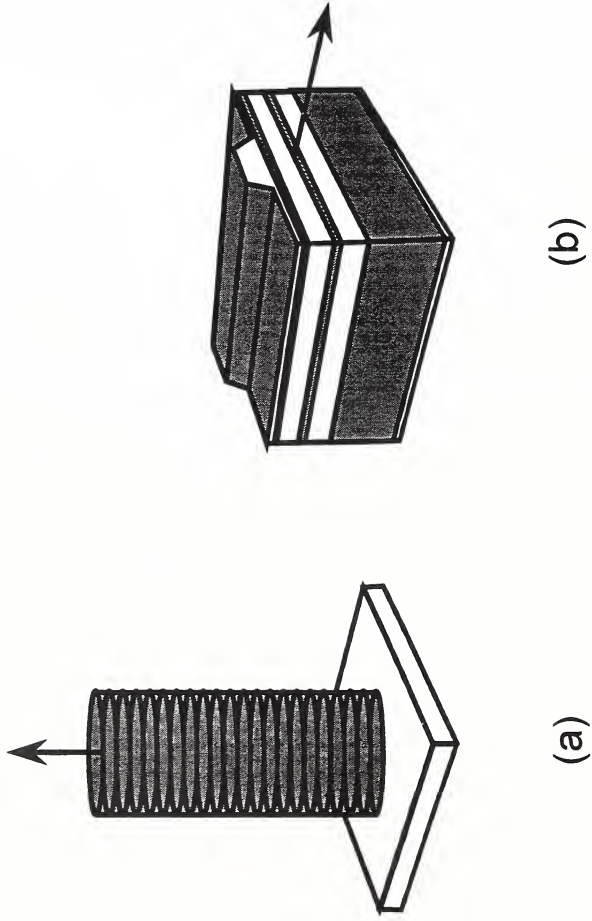
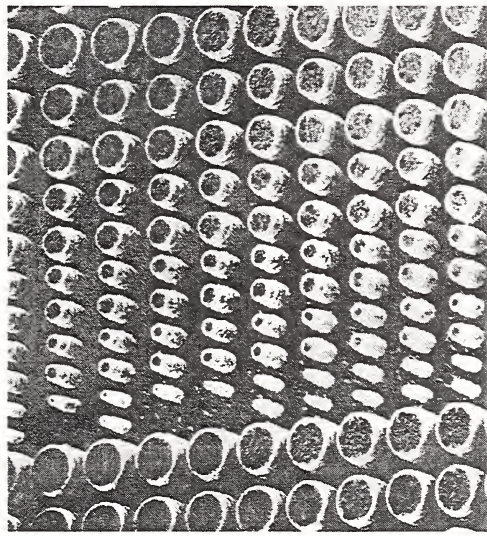
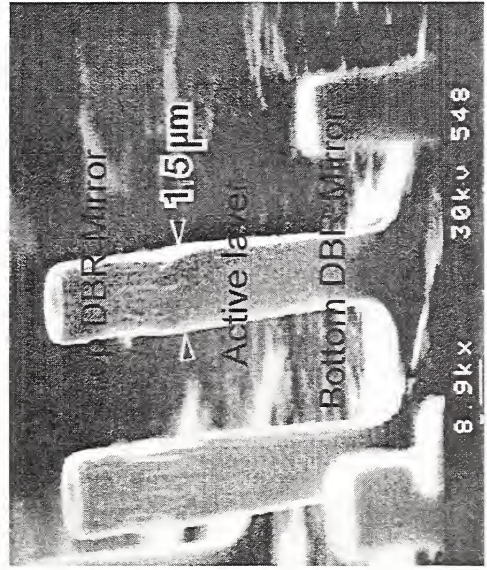


Fig. 12.1. (a) Vertical cavity surface-emitting microlaser ; (b) edge-emitting diode laser (Reprinted from Ref. [4] by Jewell et al).



(a)



(b)

Fig. 12.2. Scanning electron micrographs of vertical cavity surface-emitting microcavities (VCSEL's, SELDA's or microcavities) (Reprinted from Ref. [4] by Jewell et al).

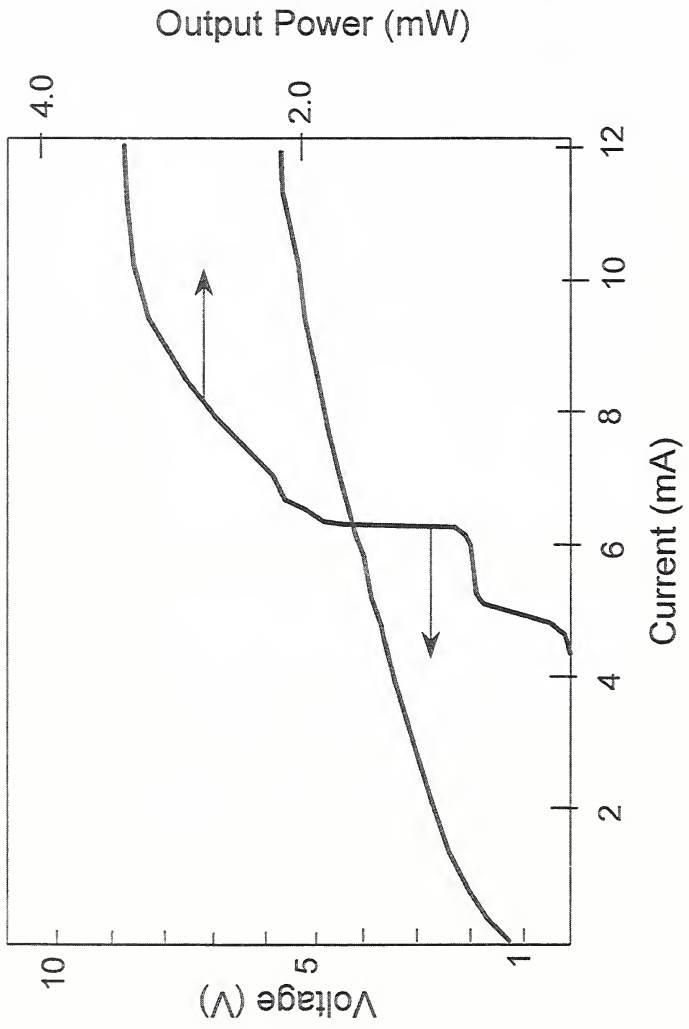
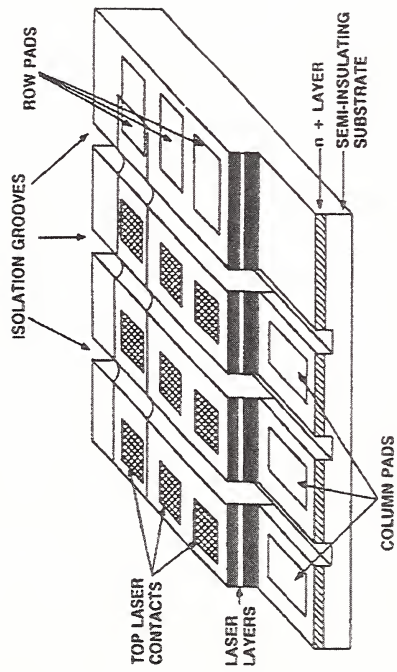
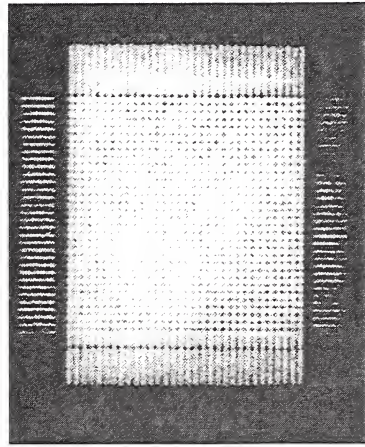


Fig. 12.3. L-I (Light output power vs. current) and V-I (Voltage vs. current) curves of a typical microlaser. (Reprinted with permission from Ref. [18] by Morgan et al. (© 1993 IEEE).



(a)



(b)

Fig. 12.4. Matrix addressing of a microlaser array. (Reprinted with permission from Ref. [28] by Orenstein et al., © 1991 IEEE)

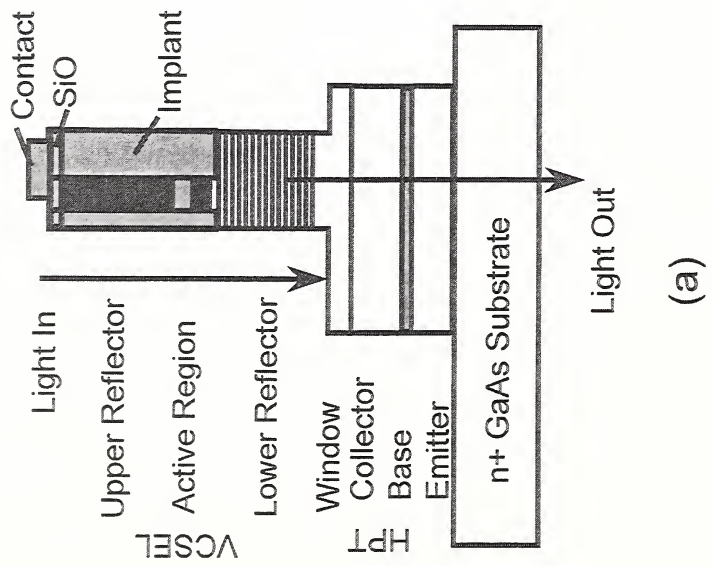


Fig. 12.5. Optically addressable integrated SELDA. (a) structure of the device, (b) light-output versus light-input relationship. (Reprinted with permission from Ref. [30] by CHAN ET AL, APPLIED PHYSICS LETTERS, 58 (21), pp. 2342-2344, 1991. © 1991 American Institute of Physics)

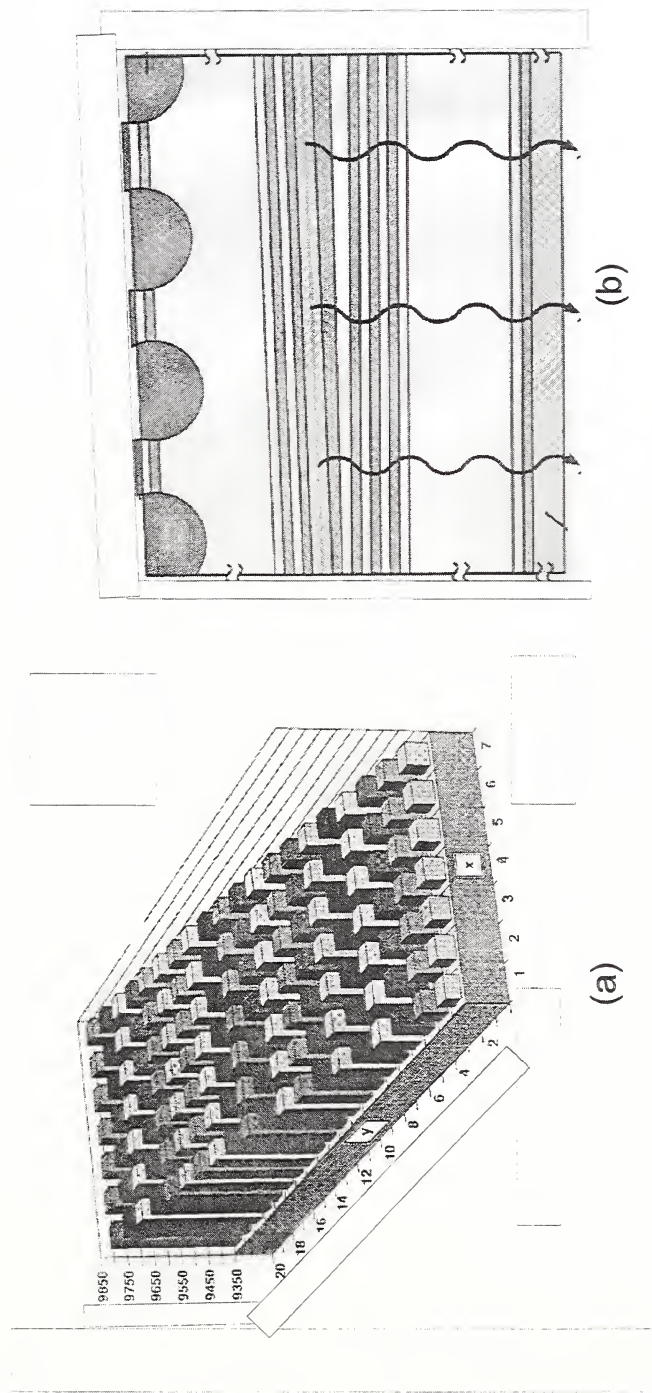


Fig. 12.6. 2-D MC-SELDA. (a) device; (b) wafer. (Reprinted with permission from Ref. [36] by Chang-Hasnain et al., © 1991 IEEE)

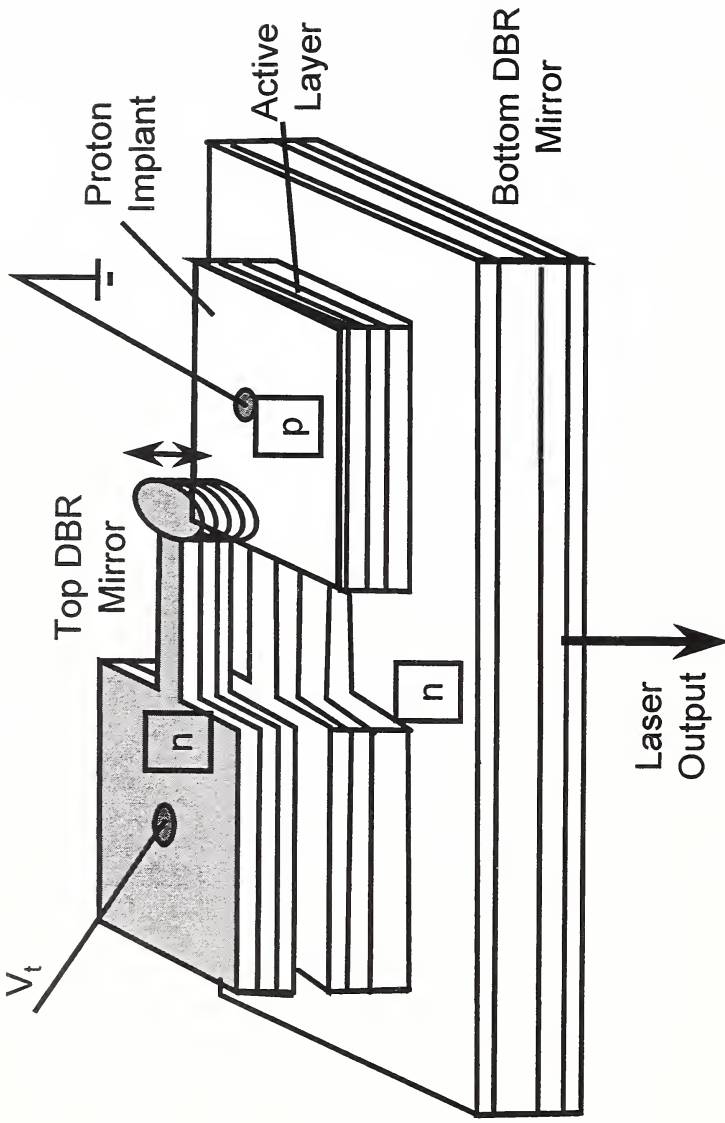


Fig. 12.7. Wavelength tuning of a microcavity laser by a deformable membrane mirror (Reprinted with permission from Ref. [38] by Wu et al, © 1991 IEE)

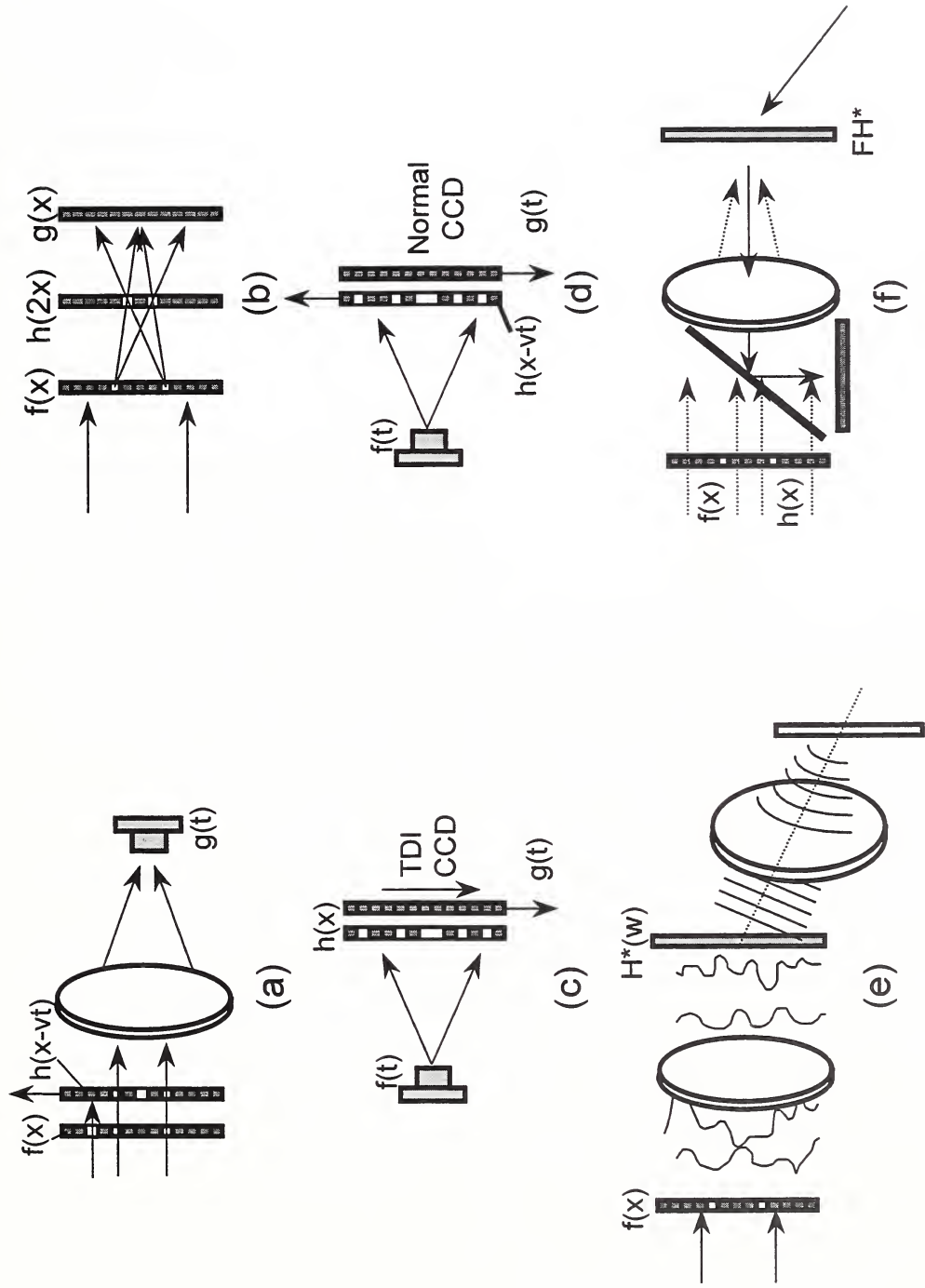


Fig. 12.8. Classification of optical correlators. TDI; time delay and integration

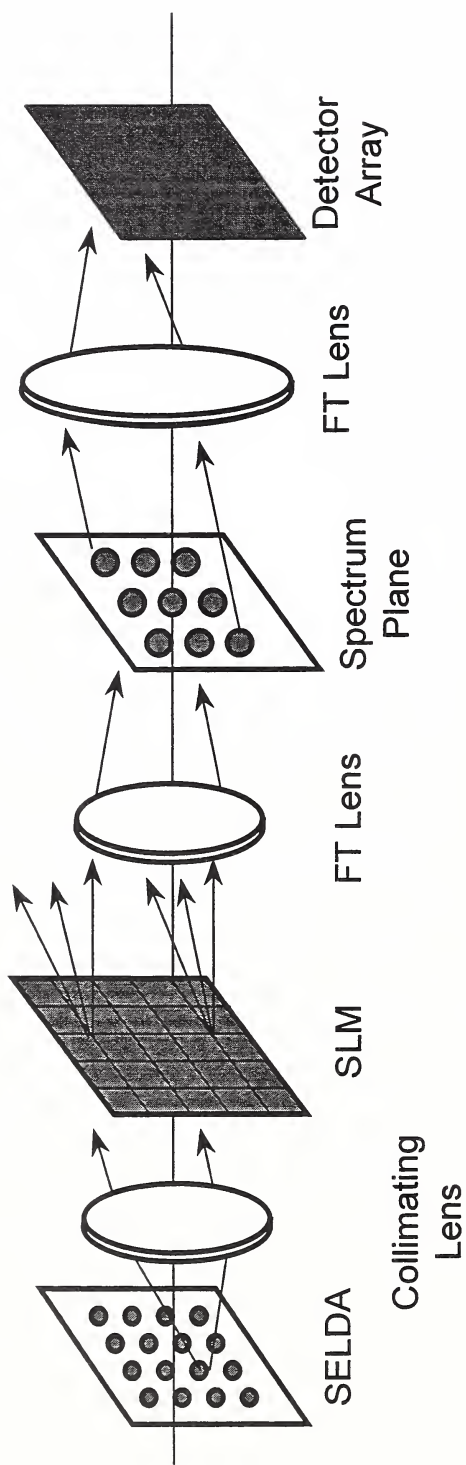
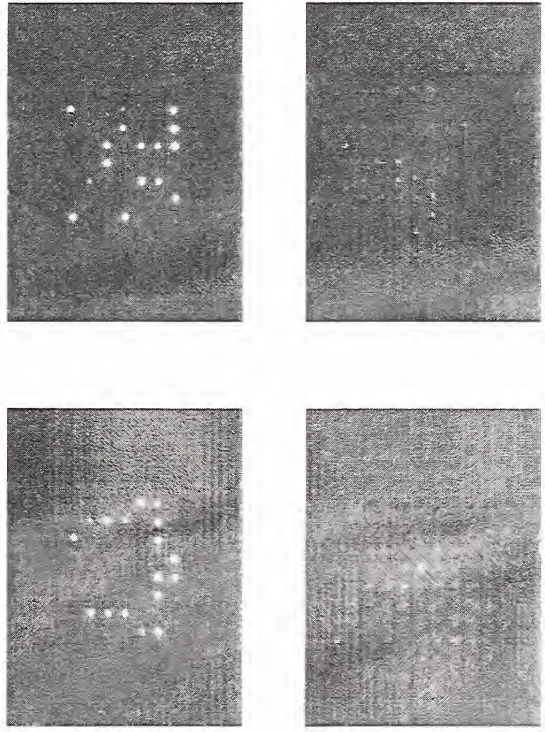
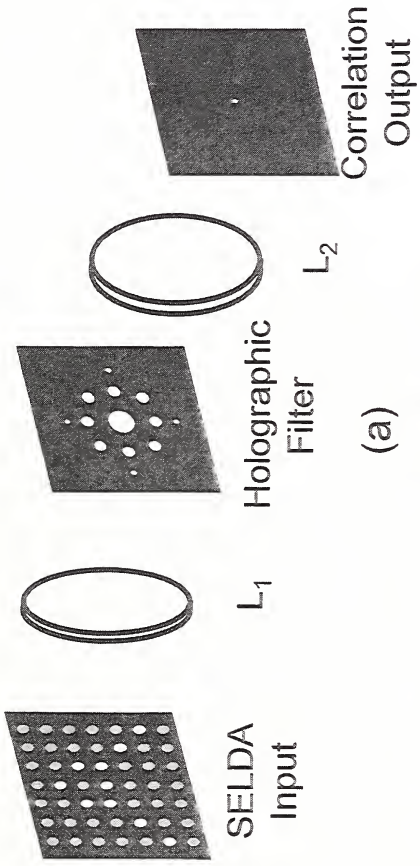


Fig. 12.9. Multichannel optical correlator with a mutually incoherent microlaser array. FT, Fourier transform. (Reprinted from Ref. [66] by Yang and Gregory, © 1995 Optical Society of America).

Fig. 12.10. Compact and robust incoherent correlator (a) system, (b) experimental results.



(a)

(b)

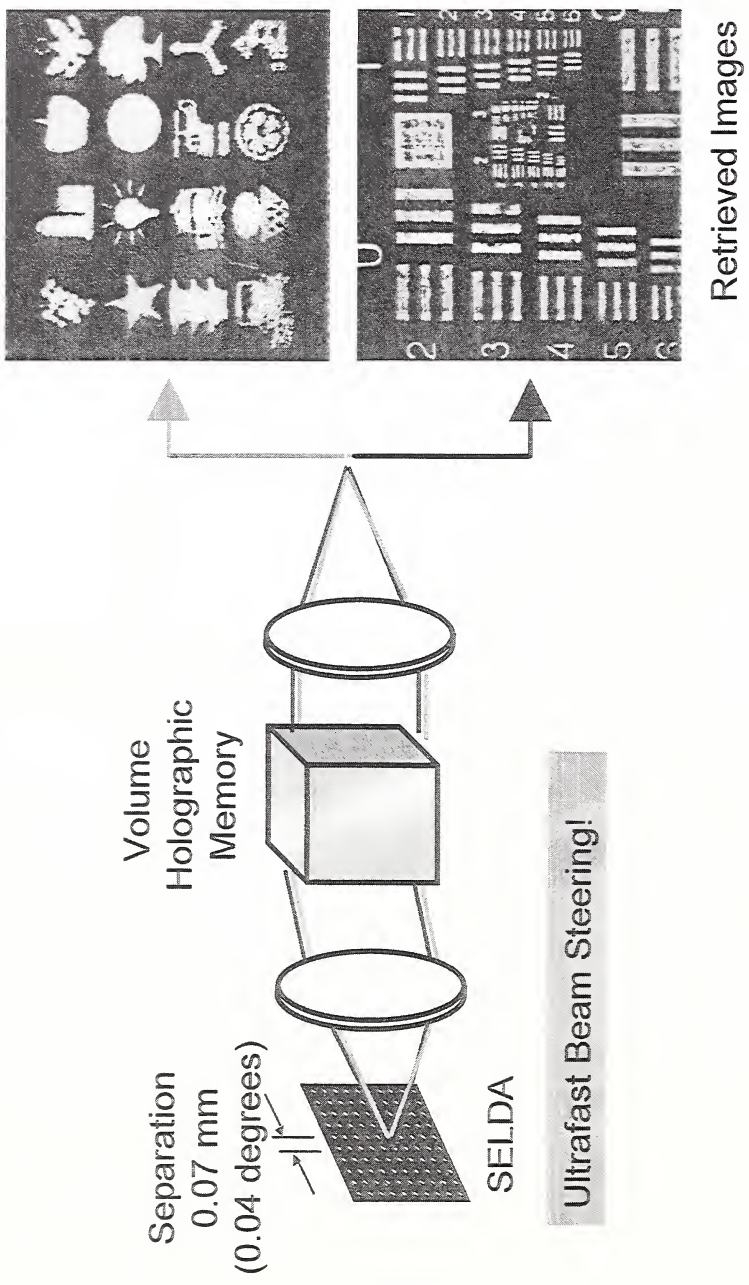
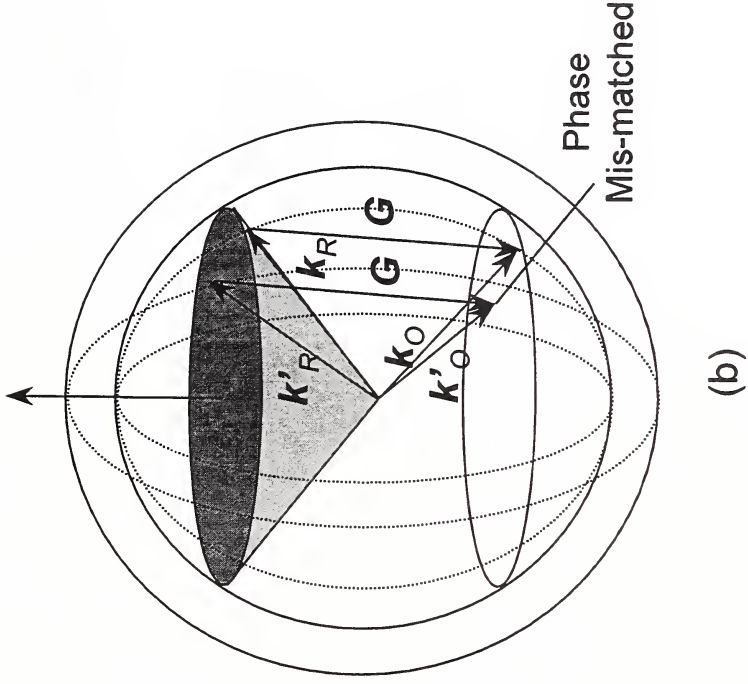
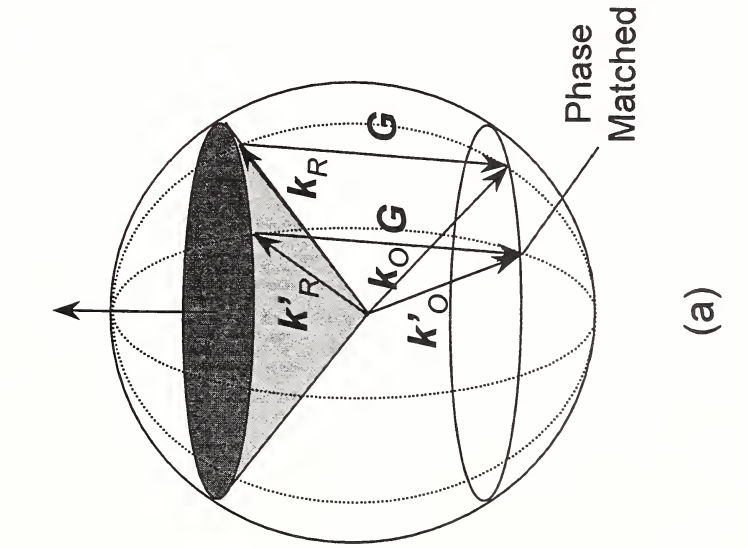


Fig. 12.11. Compact and ultrafast holographic memory with a microlaser array.



(a)



(b)

Fig. 12.12. Breaking degeneracy by use of multiple wavelengths

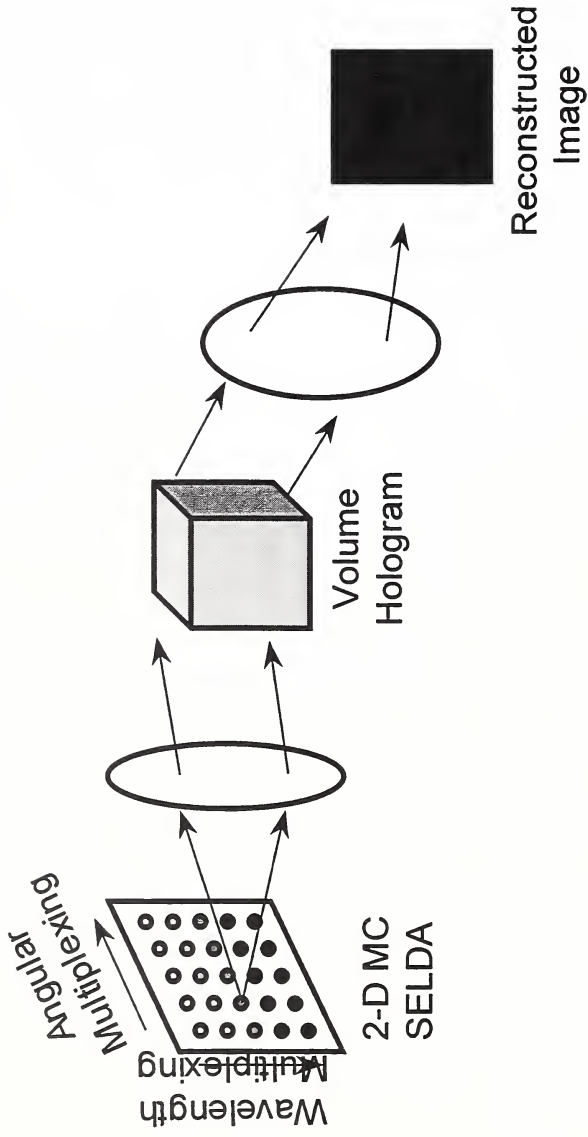


Fig. 12.13. Compact and ultrafast holographic memory readout with 2-D (Angle + Wavelength) multiplexing by a 2-D MC-SELDA.

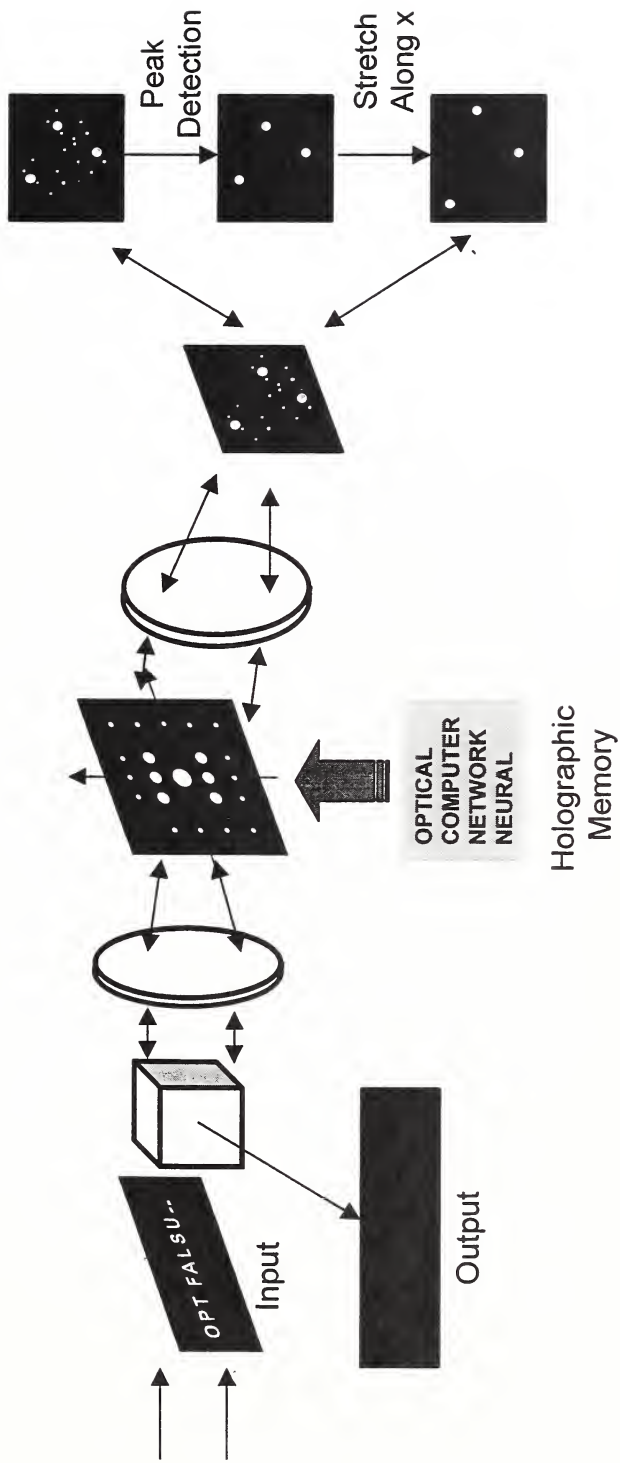


Fig. 12.14. Holographic associative memory for word-break recognition

Fig. 12.15. Holographic memory readout using an array of holographic neurons. (a) system, (b) experimental results

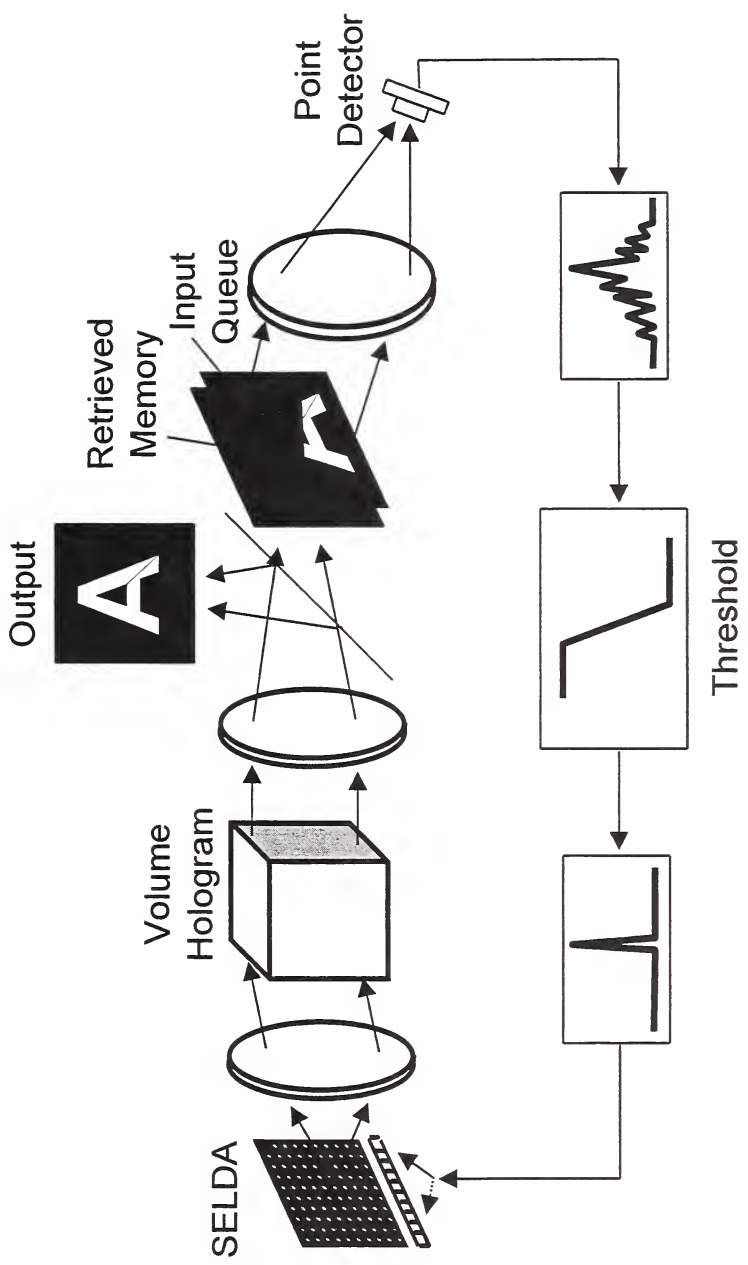


Fig. 12.16. Time division multiplexing (TDM) - based holographic associative memory with a SELDA.

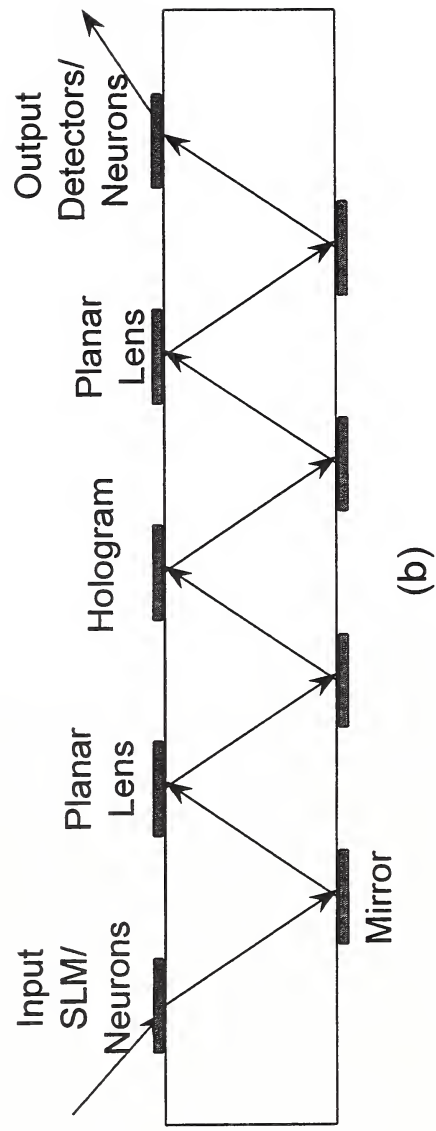
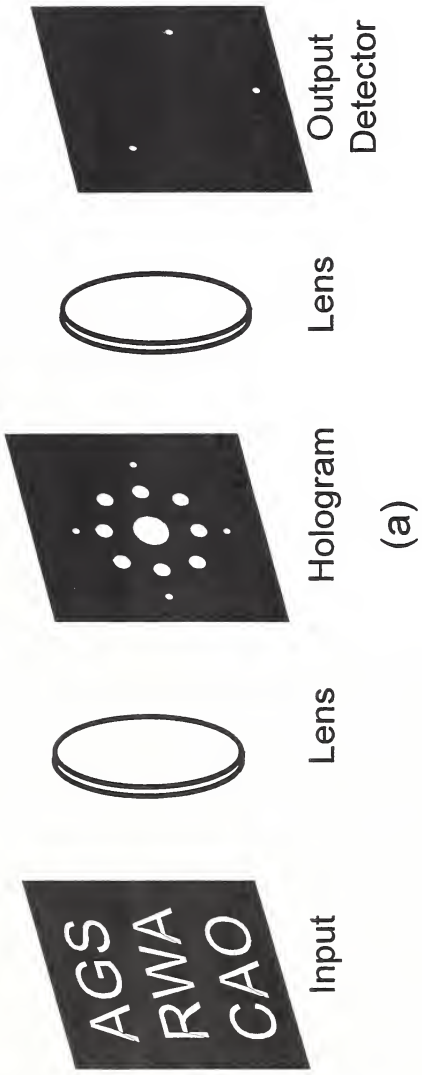


Fig. 12.17. Planar integration of a coherent optical processor (a) coherent optical processor; (b) planar integration. (Reprinted from Ref. [86] by Jahns et al. © 1995 Optical Society of America).

